Structural Engineering and Mechanics, Vol. 4, No. 5 (1996) 553-568
DOI: http://dx.doi.org/10.12989/sem.1996.4.5.553

Exact calculation of natural frequencies of repetitive structures

F.W. Williams†, D. Kennedy‡, Gaofeng Wu‡† and Jianqing Zhou‡‡

Division of Structural Engineering, School of Engineering, University of Wales Cardiff, Cardiff CF2 1XH, U.K.

Abstract. Finite element stiffness matrix methods are presented for finding natural frequencies (or buckling loads) and modes of repetitive structures. The usual approximate finite element formulations are included, but more relevantly they also permit the use of 'exact finite elements', which account for distributed mass exactly by solving appropriate differential equations. A transcendental eigenvalue problem results, for which all the natural frequencies are found with certainty. The calculations are performed for a single repeating portion of a rotationally or linearly (in one, two or three directions) repetitive structure. The emphasis is on rotational periodicity, for which principal advantages include: any repeating portions can be connected together, not just adjacent ones; nodes can lie on, and members along, the axis of rotational periodicity; complex arithmetic is used for brevity of presentation and speed of computation; two types of rotationally periodic substructures can be used in a multi-level manner; multi-level non-periodic substructuring is permitted within the repeating portions of parent rotationally periodic structures or substructures and; all the substructuring is exact, i.e., the same answers are obtained whether or not substructuring is used. Numerical results are given for a rotationally periodic structure by using exact finite elements and two levels of rotationally periodic substructures. The solution time is about 500 times faster than if none of the rotational periodicity had been used. The solution time would have been about ten times faster still if the software used had included all the substructuring features presented.

Key words: vibration; natural frequencies; space frames; periodic structures; multi-level substructuring.

1. Introduction

Theory and results are given principally for finding natural frequencies and modes of vibration of rotationally periodic structures, e.g. see Fig. 1, with comments on structures that are linearly repetitive in one, two or three Cartesian directions. The methods can be used with traditional approximate finite elements, but more importantly they can also be used with the 'exact finite elements' obtained by solving differential equations which include the member mass, to obtain element (or member) stiffnesses that are transcendental functions of the circular frequency ω (Howson *et al.* 1983, Williams and Wittrick 1983, Capron and Williams 1988, Lundén and Åkesson 1983). The vibration methods presented become buckling ones if a load factor replaces ω as the eigenparameter and permit exact multi-level substructuring, e.g., slave displacement approxi-

† Professor and Head
‡ Dr., Lecturer
‡† Dr., Now at University of Surrey, U.K.
‡‡ Dr., Now at Oxford University, U.K.

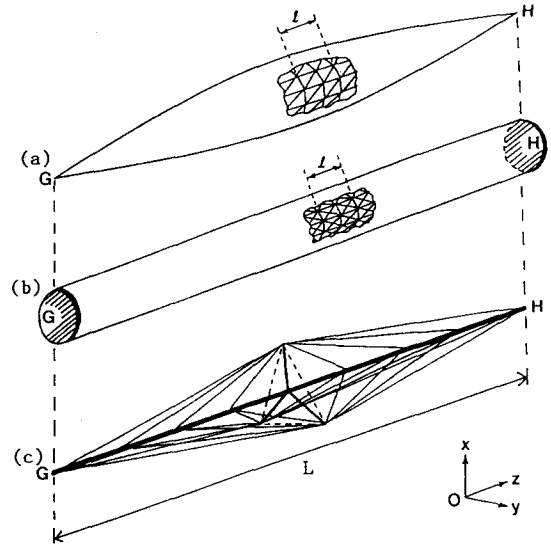

Fig. 1 Three illustrative rotationally periodic structures or substructures.

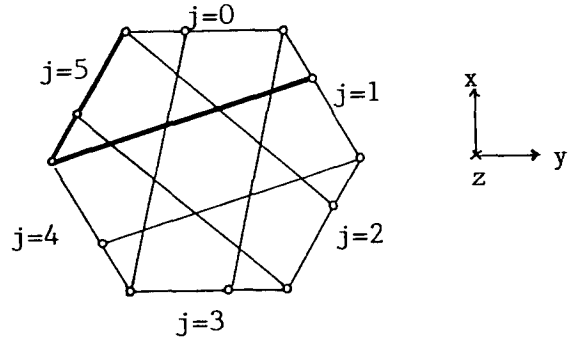

Fig. 2 Plane cross-section, with $R=6$: circles are nodes; lines are members; and the repeating portion is shown bold.

mations are absent.

Earlier derivations for rotationally periodic structures (Williams 1986a) and substructures (Williams 1986b) are unified, by using a single notation, simplified, and have been coded. Illustrative numerical results are given for a structure with rotationally periodic substructures.

Fig. 1 shows three rotationally periodic structures, with $R(>2)$ identical repeating portions, each of which is rotated about the axis by $2\pi/R$ relative to its neighbours. Lines in the areas of detail of Figs. 1(a,b) can be boundaries of triangular finite elements, representing a solid or thin-walled structure, or may be beam-column members represented exactly, so that a single element per member gives exact results. For space frames the nodes and members need not all lie on the surface, e.g., see Fig. 1(c) and Fig. 2, which shows a cross-section which illustrates that members can connect each repeating portion to any other.

Classes *A* and *B* (Williams 1986b) rotationally periodic substructures are covered, with the simpler class *B* considered first. A class *B* substructure can be connected end to end, at any

number of nodes, to any parent structure or substructure which shares its rotational periodicity, i.e., its value of R and axis. Multi-level substructuring is allowed. Hence the length l on Figs. 1 (a,b) can form a substructure, with the degrees of freedom of the internal ring of nodes eliminated by substructuring. For Fig. 1 (b), using two such substructures forms a substructure of length $2l$. Multi-level use of such doubling up can generate various lengths L of the structure shown.

A class A substructure is connected to its parent structure, which need not be rotationally periodic, only at one node at each end of its axis, i.e., at G and H on Fig. 1. For Fig. 1(b), G and H are at the centres of the shaded areas, which are e.g., rigid end caps, or frames or finite element models which share the rotational periodicity of the substructure. Fig. 1(c) is a 'stayed column' with core GH, three equally spaced central spokes, and the 24 stays and three battens (shown dashed) which the spokes pretension.

Numerous papers cover either static or dynamic analysis of rotationally periodic three dimensional structures by various methods (e.g., Thomas 1979, MacNeal *et al.* 1973, Wildheim 1981, Henry and Ferraris 1983, Leung 1980, McDaniel and Chang 1980, Anderson 1982 and Balasubramanian *et al.* 1991). However, except for those based on Williams (1986 a,b), they omit some or most of the following advantages of the present paper:

(1) the stiffness matrix method is used;
(2) exact finite elements are permitted;
(3) all natural frequencies are found with certainty;
(4) the repeating portion need not have a reflective plane of symmetry;
(5) inter-connections are permitted between any repeating portions, e.g., not just at the interface between adjacent portions;
(6) nodes can lie on, and members along, the axis;
(7) complex arithmetic is used for concise presentation and fast computation;
(8) multi-level substructuring is permitted within the repeating portion of a rotationally periodic structure or substructure and
(9) multi-level use of class A and class B rotationally periodic substructures is allowed.

Because it is crucial to (2), (3), (8) and (9) above, the next section presents the algorithm used to find all natural frequencies of non-repetitive structures with certainty. The following two sections then extend the theory and algorithm to cover first rotationally periodic structures and then substructures which have axis nodes or members.

An available computer program, BUNVIS-RG (Anderson and Williams 1987), with many of the above features has been applied (Anderson and Williams 1986, Capron *et al.* 1987). However, the only rotationally periodic substructures permitted are stayed columns with no battens. The results given below use a newer version of BUNVIS-RG which permits multi-level class A substructuring and show that such substructuring can reduce solution times by two orders of magnitude.

2. Algorithm for finding natural frequencies with certainty

This paper uses the following general algorithm (Williams and Wittrick 1983, Wittrick and Williams 1971) for finding with certainty the eigenvalues, i.e., natural frequencies or critical load factors, of any non-repetitive structure. J_T, the number of eigenvalues lying between zero and a trial ω (or load factor, Wittrick and Williams 1973a) is given by Eq. (1).

$$J_T=\sum_T J_s+\sum_T J_m+s\{\boldsymbol{K}_T\} \tag{1}$$

$$\boldsymbol{K}_T\boldsymbol{D}_T=\boldsymbol{P}_T(=\boldsymbol{0}) \tag{2}$$

Here: subscript T denotes the total parent structure, with summations over, respectively, all the substructures and all the elements or members (excluding those within substructures) of the total structure; J_s (J_m) is the number of natural frequencies of the substructure (element) that would be exceeded if it were clamped at its points of attachment to the parent structure; $\boldsymbol{K}_T$ is the dynamic overall stiffness matrix assembled from the substructure and element stiffness matrices and so is a transcendental function of ω when exact finite elements are used, and $s\{\boldsymbol{K}_T\}$ is the sign count of $\boldsymbol{K}_T$, which equals the number of negative elements on the leading diagonal of $\boldsymbol{K}_T^{\Delta}$, the upper triangular matrix obtained from $\boldsymbol{K}_T$ by the form of Gauss elimination in which multiples of the pivotal row are subtracted from unscaled succeeding rows.

$\boldsymbol{K}_T$ relates the amplitudes, $\boldsymbol{D}_T$, of the sinusoidally varying displacements $\boldsymbol{D}_T \sin \omega t$ to the corresponding force amplitudes $\boldsymbol{P}_T$ via Eq. (2), where the alternative null right-hand side is the condition for free vibration.

Many problems do not involve substructures, so that $\boldsymbol{D}_T$ contains all the degrees of freedom of the nodes of the structure and the first summation of Eq. (1) is omitted. Otherwise, $\boldsymbol{D}_T$ contains a subset of the degrees of freedom of the total structure chosen such that clamping them reduces the structure to a set of independent substructures and elements which are clamped at their attachments to the parent structure. Then the first summation of Eq. (1) and the assembly of $\boldsymbol{K}_T$ require prior knowledge of J_s and the stiffness matrix, $\boldsymbol{k}_s$, for each substructure, which are readily found as follows.

The displacement (force) amplitude vector of the substructure is ordered so that internal amplitudes, $\boldsymbol{D}_i(\boldsymbol{P}_i)$, precede the connection amplitudes, $\boldsymbol{D}_c(\boldsymbol{P}_c)$. The overall substructure stiffness matrix is assembled as if it were $\boldsymbol{K}_T$, so that partitioning it gives Eq. (3) in which T=transpose.

$$\begin{bmatrix} \boldsymbol{K}_{ii} & \boldsymbol{K}_{ic} \\ \boldsymbol{K}_{ic}^T & \boldsymbol{K}_{cc} \end{bmatrix} \begin{bmatrix} \boldsymbol{D}_i \\ \boldsymbol{D}_c \end{bmatrix} = \begin{bmatrix} \boldsymbol{P}_i \\ \boldsymbol{P}_c \end{bmatrix} = \begin{bmatrix} 0 \\ \boldsymbol{P}_c \end{bmatrix} \tag{3}$$

$$\begin{bmatrix} \boldsymbol{K}_{ii}^{\Delta} & \boldsymbol{K}_{ic}^{*} \\ \boldsymbol{0} & \boldsymbol{k}_s \end{bmatrix} \begin{bmatrix} \boldsymbol{D}_i \\ \boldsymbol{D}_c \end{bmatrix} = \begin{bmatrix} \boldsymbol{0} \\ \boldsymbol{P}_c \end{bmatrix} \tag{4}$$

Arresting Gauss elimination after the last row in $\boldsymbol{K}_{ii}$ has been pivotal gives Eq. (4) in which $\boldsymbol{k}_s$ is the required stiffness matrix because $\boldsymbol{k}_s\boldsymbol{D}_c=\boldsymbol{P}_c$ for all $\boldsymbol{P}_c$. Applying Eq. (1) to the substructure gives

$$J_s=\sum J_s+\sum J_m+s\{\boldsymbol{K}_{ii}\} \tag{5}$$

where the first summation covers substructures contained by the substructure, the second summation covers elements other than those within the contained substructures, and $s\{\boldsymbol{K}_{ii}\}$ appears because $\boldsymbol{K}_{ii}$ is its stiffness matrix when the substructure is clamped at its points of attachment to its parent, i.e., $\boldsymbol{D}_c=0$.

The first summation in Eq. (5) clearly permits a recursive procedure, i.e., multi-level substructuring is possible.

Before proceeding note that when approximate finite elements are used the above relates closely to Sturm sequence methods. Thus traditional finite elements cannot vibrate when their boundaries

are clamped, so that when substructuring is not used both summations of Eq. (1) disappear, i.e., $J_T=s\{\boldsymbol{K}_T\}$. This is essentially the Sturm sequence property, because $\boldsymbol{K}_T$ then equals the static stiffness matrix minus ω^2 times the mass matrix. However even then the above exact multi-level substructuring procedure can be much more computationally efficient than the Sturm sequence methods usually employed with traditional finite elements, and so gives exactly the same answer but more quickly.

Note too that a short and attractive (Wittrick and Williams 1973b) proof of Eq. (1) starts by hypothetically applying the Sturm sequence property to Eq. (4), with an infinite number of finite elements imagined. Hence $\boldsymbol{D}_c$ contains the finite number of connection degrees of freedom of the exact finite elements and $\boldsymbol{D}_i$ represents the infinite number of internal element freedoms which exact finite element formulations retain.

3. Rotationally periodic structures without axis nodes or members

This section relates closely to work by Thomas (1979), except that the algorithm of Eq. (1) is adapted for it, enabling exact finite elements to be used. Nodes are not permitted on the axis, so nor can members lie along the axis. Fig. 3(a) illustrates such a structure which can be thought of as solid, with each repeating portion assembled from numerous finite elements. The only connections between such solid portions are at their common interfaces. Such applications are included below, but so are more general situations in which any node in a portion can be connected to any node of any other portion, e.g., as can happen for space frames. Therefore Fig. 3(a) will be interpreted as a space frame, with its members and associated joints lying within the volume that was previously considered to be solid. There will probably be numerous members and joints, but if only those few which lie in the plane of Fig. 3(b) are shown a Fig. similar to Fig. 2 results.

Figs. 2 and 3 have R repeating portions, which are identical except for rotation by an integer multiple of $\psi=2\pi/R$. The displacement coordinate systems are assumed to rotate with the portions and to be conformable, i.e., to coincide at connections between portions, as automatically happens when using cylindrical coordinates. The portions are numbered $j=0, 1, \cdots, Q(=R-1)$ on Fig. 2, on which the nodes and members assigned to portion 5 are bold.

Because of the rotational periodicity, appropriate partitioning of the stiffness matrix $\boldsymbol{K}_T$ enables Eq. (2) to be re-written as Eq. (6), in which $\boldsymbol{D}_j$ and $\boldsymbol{P}_j$ are the displacement and force amplitude

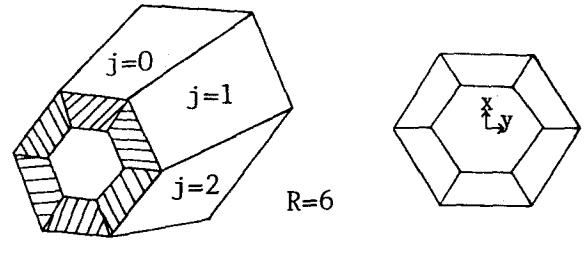

(a) (b)

Fig. 3 (a) Tapered structure with polygonal hole, (b) Typical cross-section.

vectors for the j-th portion, and the symmetry of $\boldsymbol{K}_T$ has been used.

$$\begin{bmatrix} \boldsymbol{K}_0 & \boldsymbol{K}_1 & \boldsymbol{K}_2 & \cdots & \boldsymbol{K}_Q \\ \boldsymbol{K}_Q & \boldsymbol{K}_0 & \boldsymbol{K}_1 & \cdots & \boldsymbol{K}_{Q-1} \\ \boldsymbol{K}_{Q-1} & \boldsymbol{K}_Q & \boldsymbol{K}_0 & \cdots & \boldsymbol{K}_{Q-2} \\ \vdots & \vdots & \vdots & & \vdots \\ \boldsymbol{K}_1 & \boldsymbol{K}_2 & \boldsymbol{K}_3 & \cdots & \boldsymbol{K}_0 \end{bmatrix} \begin{bmatrix} \boldsymbol{D}_0 \\ \boldsymbol{D}_1 \\ \boldsymbol{D}_2 \\ \vdots \\ \boldsymbol{D}_Q \end{bmatrix} = \begin{bmatrix} \boldsymbol{P}_0 \\ \boldsymbol{P}_1 \\ \boldsymbol{P}_2 \\ \vdots \\ \boldsymbol{P}_Q \end{bmatrix} (=\boldsymbol{0}); \qquad \begin{matrix} Q=R-1 \\ \boldsymbol{K}_{R-j}=\boldsymbol{K}_j^T \\ \boldsymbol{D}_{R+j}=\boldsymbol{D}_j \end{matrix} \tag{6}$$

$\boldsymbol{P}_T$ contains $R\times N$ force amplitudes, where N is the number of degrees of freedom of a repeating portion. Therefore it can be unambiguously represented by summing R independent force vectors which each contain only N independent force amplitudes, see Eq. (7). Eq. (7) also satisfies $P_{j+R}=P_j$, so that either of its real or imaginary parts ($i=\sqrt{-1}$) represents $\boldsymbol{P}_T$ acceptably.

$$\boldsymbol{P}_j=\sum_{h=0}^{Q}\boldsymbol{P}_{jh};\ \boldsymbol{P}_{jh}=\boldsymbol{P}_{0h}e_j^h\left(=\boldsymbol{P}_{j(R+h)}\right);\ e_j^h=\exp(ijh\psi);\ \psi=2\pi/R;\quad (j=0,\ 1,\ \cdots,\ Q) \tag{7}$$

Because of the Principle of Superposition, Eq. (6) can be solved by using each of the R harmonics $\boldsymbol{P}_{jh}$ ($h=0,\ 1,\ \cdots,\ Q$) in turn and then summing. Fortunately the solution for each harmonic has the simple form

$$\boldsymbol{D}_{jh}=\boldsymbol{D}_{0h}e_j^h \qquad (j=0,\ 1,\ \cdots,\ Q;\ h=0,\ 1,\ \cdots,\ Q) \tag{8}$$

which may be intuitively obvious, but is now proved.

Substituting Eqs. (7) and (8) in the m-th row of Eq. (6) gives

$$\left(\sum_{j=0}^{Q}\boldsymbol{K}_j e_{m+j}^h\right)\boldsymbol{D}_{0h}=\boldsymbol{P}_{0h}e_m^h, \qquad \text{i.e., } \boldsymbol{K}_{0h}\boldsymbol{D}_{0h}=\boldsymbol{P}_{0h}(=\boldsymbol{0}) \qquad (h=0,\ 1,\ \cdots,\ Q) \tag{9}$$

$$\text{with } \boldsymbol{K}_{0h}=\sum_{j=0}^{Q}\boldsymbol{K}_j e_j^h \tag{10}$$

Since Eq. (9) is independent of m, it satisfies all the rows of Eq. (6). Therefore instead of solving Eq. (6), Eq. (9) can be solved separately for each h. This is preferable because the order of $\boldsymbol{K}_{0h}$ equals the number of degrees of freedom in only one repeating portion.

Therefore the form of $\boldsymbol{K}_{0h}$ is now considered in more detail, and it is shown that computation need not be performed for all the h given by Eq. (9). Let

$$h'=\text{int}\{R/2\};\ q'=\text{int}\{(R-1)/2\} \tag{11}$$

Thus h' and q' are the highest integers that do not exceed $R/2$ and $(R-1)/2$, respectively, and $(h'-q')=0(1)$ for R odd (even). In addition, $e_{R-j}^h=e_j^{-h}$ and Eq. (6) gives $K_{R-j}=K_j^T$, so that $K_{R-j}e_{R-j}^h=(K_j e_j^h)^H$, where H denotes Hermitian transpose. Hence Eq. (10) gives

$$\begin{aligned}\boldsymbol{K}_{0h}&=\boldsymbol{K}_0+(h'-q')\,\boldsymbol{K}_{h'}\cos(h\pi)+\sum_{j=1}^{q'}(\boldsymbol{K}_j e_j^h+\boldsymbol{K}_{R-j}e_{R-j}^h)\\ &=\boldsymbol{K}_0+(h'-q')\,\boldsymbol{K}_{h'}\cos(h\pi)+\sum_{j=1}^{q'}\{\boldsymbol{K}_j e_j^h+(\boldsymbol{K}_j e_j^h)^H\}\end{aligned} \tag{12}$$

Here $\boldsymbol{K}_0$ and $\boldsymbol{K}_{h'}\cos(h\pi)$ are both clearly real and symmetric. So is the summation if $h=0$, or if R is even and $h=R/2$, but otherwise it is complex and Hermitian. Hence

$$\boldsymbol{K}_{0h} \text{ is } \left\{ \begin{array}{l} \text{real and symmetric } (h=0, \text{ and } h=R \text{ if } R/2 \text{ even}) \\ \text{Hermitian } (h=1, 2, \cdots, q') \end{array} \right\} \tag{13}$$

and $\boldsymbol{K}_{0(R-h)}=\overline{\boldsymbol{K}}_{0h}$, where the overbar denotes complex conjugate. Thus, with $\boldsymbol{P}_{0(R-h)}$ chosen appropriately, Eqs. (9) and (10) give

$$\boldsymbol{P}_{0(R-h)}=\overline{\boldsymbol{P}}_{0h};\ \boldsymbol{K}_{0(R-h)}=\overline{\boldsymbol{K}}_{0h};\ \boldsymbol{D}_{0(R-h)}=\overline{\boldsymbol{D}}_{0h}\ (h=1, 2, \cdots, q') \tag{14}$$

Hence Eq. (9) need only be performed for $h=0, 1, \cdots, h'$.

$\boldsymbol{P}_T=0$ for free vibrations. Hence Eq. (7) gives $\boldsymbol{P}_{0h}=\boldsymbol{0}$ and so all natural frequencies and modes of the total structure can be found much more efficiently by solving Eq. (15).

$$\boldsymbol{K}_{0h}\boldsymbol{D}_{0h}=\boldsymbol{0} \tag{15}$$

$$J_h=\sum J_{sh}+\sum J_s+\sum J_m+s\{\boldsymbol{K}_{0h}\} \qquad (h=0, 1, \cdots, h') \tag{16}$$

Because Eqs. (2) and (15) are analogous, it might seem obvious that the algorithm of Eq. (1) extends to Eq. (15) to give Eq. (16), as was proved by Williams (1986 a,b). In Eq. (16): the summations cover a single repeating portion for all class *B* substructures, all other substructures, and elements not within substructures; J_s and J_m still have the meanings given beneath Eq. (1), the subscript h of J_{sh} indicates that the h of the substructure is the same as for its parent structure (i.e., of J_h) when calculating how many of its natural frequencies would be exceeded if its connection freedoms $\boldsymbol{D}_c$ were to be clamped; and $s\{\boldsymbol{K}_{0h}\}$ is the sign count of $\boldsymbol{K}_{0h}$, calculated precisely as described beneath Eq. (1), noting that for any Hermitian matrix, e.g., $\boldsymbol{K}_{0h}$, the leading diagonal of its upper triangular form, e.g., of $\boldsymbol{K}^{\Delta}_{0h}$, is real and so its negative elements can still be counted.

Eq. (5) and related text give J_s and $\boldsymbol{k}_s$ for substructures, with the latter being assembled into $\boldsymbol{K}_{0h}$ by the usual finite element procedure. J_{sh} and $\boldsymbol{k}_{sh}$ can be found similarly, except that $\boldsymbol{K}_{0h}$ is the matrix partitioned by Eq. (3).

Note that whenever Eq. (13) shows that $\boldsymbol{K}_{0h}$ is Hermitian (i.e., $h=1, 2, \cdots, q'$), the natural frequencies form coincident pairs and J_h is the number of such pairs exceeded by the trial frequency. Hence the total number of natural frequencies exceeded, J_h^*, is given by

$$J_h^*=\alpha_h J_h; \qquad \alpha_h \left\{ \begin{array}{l} =1\ (h=0, \text{ or } h=R/2 \text{ if } R \text{ even}) \\ =2\ (h=1, 2, \cdots, q'). \end{array} \right\} \tag{17}$$

Ways of seeing why the natural frequencies which appear in pairs do so include the following. Firstly, Eq. (14) showed that solutions of Eq. (15) for which $h=1, 2, \cdots, q'$ represent two solutions, for h and $R-h$. Secondly, the modes given by the real and imaginary parts of the $\boldsymbol{D}_{0h}$ obtained by solving Eq. (15) differ unless $\boldsymbol{K}_{0h}$ is real. Thirdly, writing Eq. (15) in real arithmetic replaces $\boldsymbol{K}_{0h}$ by a matrix of twice the order and for which the diagonal elements of $\boldsymbol{K}^{\Delta}_{0h}$ are readily seen to appear in identical pairs. Finally, Fig. 4 illustrates an important physical reason, as follows. Eq. (8) gives the mode. Because of the periodicity, an alternative mode obviously results from rotating this mode round the structure by an angle ψ. When observed from a fixed viewpoint, these two modes are identical when $h=0$, or when $h=R/2$ and R is even, their amplitudes being equal in the former case and equal and opposite for the latter case. For all other h (i.e. 1, 2, $\cdots$, q') the two modes differ, but combining them in suitable proportions gives the apparently different modes obtained by rotating the first mode by $m\psi$ ($m=2, 3, \cdots, Q$), which

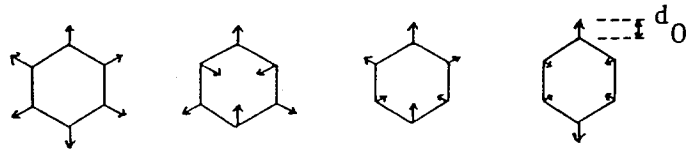

(a) Unrotated mode,

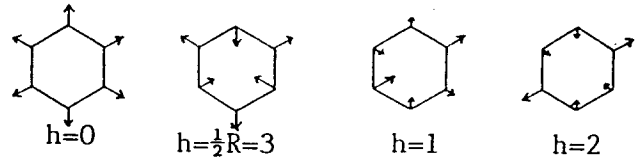

(b) Mode rotated by $\pi/3$.

Fig. 4 Radial displacements of modes, =real part of $d_j=d_0 e_j^h$ for hexagon ($R=6$). d_0 is real and the arrow lengths indicate the displacements ($=\pm d_0$ or $\pm d_0/2$). The tangential displacements are not shown. Node zero, at the top of the hexagon, is the viewpoint.

is why $\alpha_h=2$, not $\alpha_h=R$.

As an indication that Eq. (17) is correct, consider any rotationally periodic substructure with no substructures and with all its nodes clamped, i.e., $\boldsymbol{D}_T=\boldsymbol{0}$. This can be achieved by removing from $\boldsymbol{K}_T$ all those rows and columns corresponding to the clamps. Hence, $\boldsymbol{K}_T$ disappears, so that $s\{\boldsymbol{K}_T\}=0$ and Eq. (1) gives

$$J_T=\sum_T J_m \tag{18}$$

Alternatively, J_T can be found as the sum of the values of J_h^* for the subproblems of Eq. (15). Because $s\{\boldsymbol{K}_{0h}\}=0$ for the same reason that $s\{\boldsymbol{K}_T\}=0$, Eqs. (16) and (17) give

$$\left.\begin{aligned} J_T=\sum_{h=0}^{h'}\alpha_h J_h=(\sum J_m)\left(\sum_{h=0}^{h'}\alpha_h\right)=(\sum J_m)\left(1+\sum_{h=1}^{h'}2\right)=R\sum_{h=1}^{h'}J_m \quad (R \text{ odd})\\ =(\sum J_m)\left(1+\sum_{h=1}^{q'}2+1\right)=R\sum J_m \quad (R \text{ even}) \end{aligned}\right\} \tag{19}$$

Since $\sum J_m$ is for one repeating portion and $\sum_T J_m$ ($=R\sum J_m$) is for the total structure, the required indication is that Eqs. (18) and (19) both give J_T the same value.

4. Inclusion of axis nodes and members

The theory is now extended to include nodes on the axis and members (or class A substructures) lying along it, i.e., axis nodes and axis members.

Let every axis node be replaced by R split axis nodes, equally spaced round an infinitesimally small circle and belonging to each of the R repeating portions, see Fig. 5. Split axis members connect such nodes and have the length of the real axis members but $(1/R)$-th of their other properties, e.g., of EA, EI, mass per unit length, axial force, etc.. Thus fusing the axis nodes and members of the R portions together gives the original structure.

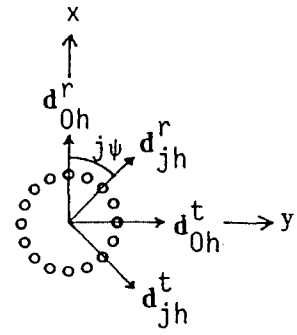

Fig. 5 Split axis nodes, for $R=16$ and $j=2$.

Denote the displacements of all split axis nodes of the j-th portion, see Fig. 5, by $\boldsymbol{d}^r_{jh}$; $\boldsymbol{d}^t_{jh}$ and $\boldsymbol{d}^z_{jh}$ where $\boldsymbol{d}^w_{jh}$ ($w=r$, t or z) contains the translations along, and rotations about, the w axis. Using $\boldsymbol{p}^w_{jh}$ to denote the corresponding forces, and ordering and partitioning Eq. (15) gives

$$\begin{bmatrix} \boldsymbol{K}_h^{uu} & \boldsymbol{K}_h^{ur} & \boldsymbol{K}_h^{ut} & \boldsymbol{K}_h^{uz} \\ & \boldsymbol{k}_h^{rr} & \boldsymbol{k}_h^{rt} & \boldsymbol{k}_h^{rz} \\ & & \boldsymbol{k}_h^{tt} & \boldsymbol{k}_h^{tz} \\ & \text{Hermitian} & & \boldsymbol{k}_h^{zz} \end{bmatrix} \begin{bmatrix} \boldsymbol{D}^u_{0h} \\ \boldsymbol{d}^r_{0h} \\ \boldsymbol{d}^t_{0h} \\ \boldsymbol{d}^z_{0h} \end{bmatrix} = \begin{bmatrix} \boldsymbol{P}^u_{0h} \\ \boldsymbol{p}^r_{0h} \\ \boldsymbol{p}^t_{0h} \\ \boldsymbol{p}^z_{0h} \end{bmatrix} \tag{20}$$

where $\boldsymbol{D}^u_{0h}$ contains the displacements of all nodes not on the axis.

Eq. (8) gives $\boldsymbol{d}^r_{jh}=\boldsymbol{d}^r_{0h}e^h_j$, $\boldsymbol{d}^t_{jh}=\boldsymbol{d}^t_{0h}e^h_j$, and $\boldsymbol{d}^z_{jh}=\boldsymbol{d}^z_{0h}e^h_j$, and resolving displacements on Fig. 5 shows that the compatibility needed for the split axis nodes to be fused together, after deflection, to form the original structure requires that $h=1$ for $\boldsymbol{d}^r_{jh}$ and $\boldsymbol{d}^t_{jh}$ and that $h=0$ for $\boldsymbol{d}^z_{0h}$. Hence, there is one complete sine wave round the circumference ($h=1$) or the mode is either an 'axial' or 'breathing' one ($h=0$). Therefore, for $h>1$ Eq. (20) reduces to Eq. (21).

$$\boldsymbol{K}_h^{uu}\boldsymbol{D}^u_{0h}=\boldsymbol{P}^u_{0h}\ (h>1) \tag{21}$$

$$\begin{bmatrix} \boldsymbol{K}_0^{uu} & \boldsymbol{K}_0^{uz} \\ (\boldsymbol{K}_0^{uz})^H & \boldsymbol{k}_0^{zz} \end{bmatrix} \begin{bmatrix} \boldsymbol{D}^u_{00} \\ \boldsymbol{d}^z \end{bmatrix} = \begin{bmatrix} \boldsymbol{P}^u_{0h} \\ \boldsymbol{p}^z \end{bmatrix} \quad (\boldsymbol{p}^z=R\boldsymbol{p}^z_{00})\ (h=0) \tag{22}$$

in which any members with one end on the axis contribute to $\boldsymbol{K}_h^{uu}$ but have that end clamped. Similarly Eq. (22) applies for $h=0$ where $\boldsymbol{d}^z=\boldsymbol{d}^z_{00}(\boldsymbol{p}^z)$ is the total displacement (force) along the z axis because the other values of h contribute no axial displacements or forces to axis nodes. Finally, the case $h=1$ which follows is more complicated because $\boldsymbol{d}^r_{jh}$ and $\boldsymbol{d}^t_{jh}$ are related.

Dividing Eq. (8) by e^h_j gives the first of the two expressions for $\boldsymbol{d}^r_{01}$ and $\boldsymbol{d}^t_{01}$ of Eqs. (23), whereas resolution and compatibility on Fig. 5 gives the second expressions.

$$\left.\begin{aligned} \boldsymbol{d}^r_{01}&=\boldsymbol{d}^r_{j1}\cos j\psi-i\boldsymbol{d}^r_{j1}\sin j\psi=\boldsymbol{d}^r_{j1}\cos j\psi-\boldsymbol{d}^t_{j1}\sin j\psi \\ \boldsymbol{d}^t_{01}&=\boldsymbol{d}^t_{j1}\cos j\psi-i\boldsymbol{d}^t_{j1}\sin j\psi=\boldsymbol{d}^t_{j1}\cos j\psi+\boldsymbol{d}^r_{j1}\sin j\psi \end{aligned}\right\}\ (j=0,\ 1,\ \cdots,\ Q) \tag{23}$$

Since Eqs. (23) hold for all j, their solution is

$$\boldsymbol{d}_{j1}^{l}=i\boldsymbol{d}_{j1}^{r} \qquad (j=0,\ 1,\ \cdots,\ Q) \tag{24}$$

If $\boldsymbol{p}_{xh}$ and $\boldsymbol{p}_{yh}$ ($h=0,\ 1,\ \cdots,\ Q$) are total forces at the axis nodes after the split nodes are fused together, resolving on Fig. 5 and using Eq. (7) gives

$$\left.\begin{aligned}\boldsymbol{p}_{xh}&=\sum_{j=0}^{Q}(\boldsymbol{p}_{jh}^{r}\cos j\psi-\boldsymbol{p}_{jh}^{t}\sin j\psi)=\sum_{j=0}^{Q}(\boldsymbol{p}_{0h}^{r}e_{j}^{h}\cos j\psi-\boldsymbol{p}_{0h}^{t}e_{j}^{h}\sin j\psi)\\ \boldsymbol{p}_{yh}&=\sum_{j=0}^{Q}(\boldsymbol{p}_{jh}^{r}\sin j\psi+\boldsymbol{p}_{jh}^{t}\cos j\psi)=\sum_{j=0}^{Q}(\boldsymbol{p}_{0h}^{r}e_{j}^{h}\sin j\psi+\boldsymbol{p}_{0h}^{t}e_{j}^{h}\cos j\psi)\end{aligned}\right\} \tag{25}$$

Substituting the mathematical results

$$\sum_{j=0}^{Q}e_{j}^{h}\cos j\psi=\sum_{j=0}^{Q}e_{j}^{h}\sin j\psi=0 \quad (h\neq 1);\quad \sum_{j=0}^{Q}e_{j}^{1}\cos j\psi=R/2,\quad \sum_{j=0}^{Q}e_{j}^{1}\sin j\psi=iR/2 \quad (h=1) \tag{26}$$

into Eq. (25) shows the expected result that $\boldsymbol{p}_{xh}$ and $\boldsymbol{p}_{yh}$ are zero when $h\neq 1$, i.e., the only unbalanced axis forces perpendicular to the axis occur when $h=1$, i.e., external loading $\boldsymbol{p}_x$ or $\boldsymbol{p}_y$ applied at the axis and perpendicular to it causes only the $h=1$ displacement pattern of Eq. (8), so that $\boldsymbol{p}_x=\boldsymbol{p}_{x1}$ and $\boldsymbol{p}_y=\boldsymbol{p}_{y1}$. Also, when $h=1$ Eqs. (25) and (26) give

$$\boldsymbol{p}_x=\boldsymbol{p}_{x1}=(R/2)(\boldsymbol{p}_{01}^{r}-i\boldsymbol{p}_{01}^{t});\quad \boldsymbol{p}_y=\boldsymbol{p}_{y1}=i\boldsymbol{p}_x \tag{27}$$

Since $\boldsymbol{d}_{0h}^{r}$ and $\boldsymbol{d}_{0h}^{t}$ are zero except when $h=1$, $\boldsymbol{d}_{01}^{r}$ and $\boldsymbol{d}_{01}^{t}$ are the total deflections, denoted by $\boldsymbol{d}_x$ and $\boldsymbol{d}_y$ below. Hence Eq. (24) gives $\boldsymbol{d}_y=i\boldsymbol{d}_x$ and so Eq. (20) becomes

$$\begin{bmatrix}\boldsymbol{K}_1^{uu} & \boldsymbol{K}_1^{ur}+i\boldsymbol{K}_1^{ut}\\ \text{Hermitian} & R/2\{\boldsymbol{k}_1^{rr}+\boldsymbol{k}_1^{tt}+i\boldsymbol{k}_1^{rt}-i(\boldsymbol{k}_1^{rt})^{H}\}\end{bmatrix}\begin{bmatrix}\boldsymbol{D}_{01}^{u}\\ \boldsymbol{d}_x\end{bmatrix}=\begin{bmatrix}\boldsymbol{P}_{01}^{u}\\ \boldsymbol{p}_x\end{bmatrix};\quad (\boldsymbol{d}_y=i\boldsymbol{d}_x,\ \boldsymbol{p}_y=i\boldsymbol{p}_x) \tag{28}$$

The effect of the axis nodes and members is clearly to replace the $\boldsymbol{D}_{0h}$ of Eq. (15) and the $\boldsymbol{K}_{0h}$ of Eqs. (15) and (16) by the displacement vectors and stiffness matrices of Eqs. (22), (28) and (21) for, respectively, $h=0$, $h=1$ and $h>1$. However, when computing J_h from Eq. (16) (or J_{sh}, see between Eqs. (16) and (17)) the value of J_m used for axis members (or class A substructures lying along the axis) needs care, as follows. For members with no torsional-flexural coupling, J_m is the sum of J_{m0}, the number of clamped ended axial and twisting natural frequencies exceeded, and J_{m1}, the number of clamped ended flexural natural frequencies exceeded. The flexural modes occur in coincident pairs, because the rotational periodicity requires equality of the principal second moments of area for axis members, and J_{m1} includes only one of each pair. Such flexural displacements are compatible only with $h=1$, so that the α_h of Eq. (17) accounts for the modes being paired, and the axial and torsional modes are only compatible with $h=0$. Therefore, in Eq. (16),

$$J_m=J_{m0}(\text{or } J_{s0}) \quad (h=0);\quad J_m=J_{m1}(\text{or } J_{s1}) \quad (h=1);\quad J_m=0 \quad (h>1) \tag{29}$$

with terms in brackets following analogously for a class A substructure lying along the axis and J_{sh} defined between Eqs. (16) and (17).

The J_s and $\boldsymbol{k}_s$ for a class A substructure are now simply given by

$$J_s=\sum_{h=0}^{h'}\alpha_h J_{sh};\quad \boldsymbol{k}_s=\begin{bmatrix}\boldsymbol{k}_{s0} & \boldsymbol{0}\\ \boldsymbol{0} & \boldsymbol{k}_{s1}\end{bmatrix} \tag{30}$$

Here: Eq. (17) gives α_h; $\boldsymbol{k}_{s0}$ and $\boldsymbol{k}_{s1}$ are the $\boldsymbol{k}_{sh}$ ($h=0,1$) obtained by re-ordering Eqs. (22) and (28) such that those elements of, respectively, $\boldsymbol{d}^z$ and $\boldsymbol{d}_x$ relating to the axis nodes at the ends of the substructure come last and making them the $\boldsymbol{D}_c$ of Eq. (3); and J_{sh} is calculated during this process for $h=0$ and 1, and otherwise from Eq. (5) with J_s and $\boldsymbol{K}_{ii}$ replaced by J_{sh} and $\boldsymbol{K}_h^{uu}$, see Eq. (21).

The $\boldsymbol{k}_{s1}$ of Eq. (30) is not in a convenient form for assembling the stiffness matrix of the parent structure, because it is Hermitian and such that Eq. (31) holds

$$\boldsymbol{k}_{s1}\boldsymbol{d}_x^*=\boldsymbol{p}_x^*, \tag{31}$$

$$\boldsymbol{d}_y^*=i\boldsymbol{d}_x^*, \quad \boldsymbol{p}_y^*=i\boldsymbol{p}_x^* \tag{32}$$

where $\boldsymbol{d}_x^*(\boldsymbol{p}_x^*)$ is the complex subset of $\boldsymbol{d}_x(\boldsymbol{p}_x)$ obtained by excluding all axis nodes except G and H, see Fig. 1. Hence Eq. (28) gives Eq. (32). In contrast, since either the real or imaginary parts of $\boldsymbol{d}_x^*$, $\boldsymbol{d}_y^*$, $\boldsymbol{p}_x^*$ and $\boldsymbol{p}_y^*$ are the required displacement and force amplitudes needed when assembling the stiffness matrix of the parent structure, the stiffness matrix required is that corresponding either to $\{(\boldsymbol{d}_x^{*R})^T, (\boldsymbol{d}_y^{*R})^T\}^T$ or to $\{(\boldsymbol{d}_x^{*I})^T, (\boldsymbol{d}_y^{*I})^T\}$ where R and I denote real and imaginary parts. Separating the real and imaginary parts of Eq. (31), substituting from Eq. (32), and noting that $\boldsymbol{k}_{s1}^I=(-\boldsymbol{k}_{s1}^I)^T$ because $\boldsymbol{k}_{s1}$ is Hermitian, shows that these two stiffness matrices are identical, such that

$$\begin{bmatrix} \boldsymbol{k}_{s1}^R & \boldsymbol{k}_{s1}^I \\ \text{Symmetric} & \boldsymbol{k}_{s1}^R \end{bmatrix} \begin{bmatrix} \boldsymbol{d}_x^\circ \\ \boldsymbol{d}_y^\circ \end{bmatrix} = \begin{bmatrix} \boldsymbol{p}_x^\circ \\ \boldsymbol{p}_y^\circ \end{bmatrix} \tag{33}$$

in which all terms are real and $\boldsymbol{d}_x^\circ$, $\boldsymbol{d}_y^\circ$, $\boldsymbol{p}_x^\circ$ and $\boldsymbol{p}_y^\circ$ denote either the real parts of $\boldsymbol{d}_x^*$, $\boldsymbol{d}_y^*$, $\boldsymbol{p}_x^*$ and $\boldsymbol{p}_y^*$ or their imaginary parts.

When the shaded areas of Fig. 1(b) are rigid discs, exactly correct results can be obtained by using standard transformations, e.g., those of BUNVIS-RG, for offsets between member ends and the nodes to which they are connected. Thus, every member which is connected to the disc in the example below is modeled as connected to a node at the centre of the disc, with an offset equal to its radius.

5. Numerical example

The example of Figs. 6 and 7 is a structure in space, with extremely small springs added

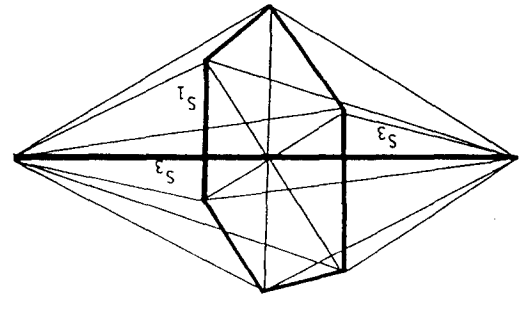

Fig. 6 Sketch of example structure, with $R=R_F(=6)$ and all detail of substructures omitted. Thin lines are pretensioned stays and thick lines are compressed substructures.

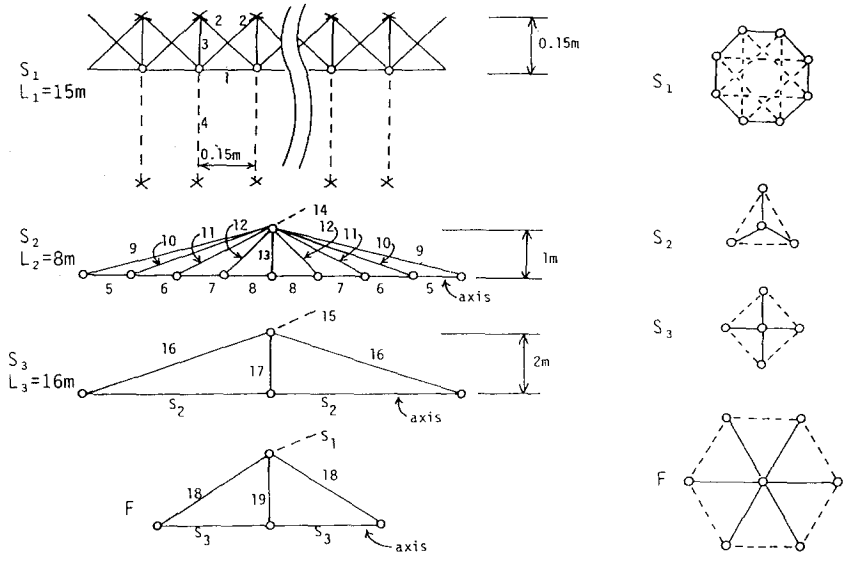

Fig. 7 Detail of the structure analysed. L denotes length and the end views are not to scale. Substructures are represented by their axis when assembling their parent substructure or structure. Nodes are indicated by circles, so that it can be seen where members are assumed to cross without touching. The end views show all nodes, but the other views show only those nodes needed when modelling a repeating portion for BUNVIS-RG, in which case nodes indicated by crosses belong to another repeating portion. The dashed lines are in their correct positions on the end views, but not on the pictures of the repeating portions. Note that the members shown dashed for S_1 connect a node to its counterpart in the next but two repeating portion. Because the S_1 form the sides of a polygon their axes are not collinear, but the small resulting geometric incompatibility where the discs are connected together is ignored as being typical of joint details usually omitted in structural analysis.

Table 1 Properties of the members. $GJ=0.8EI$ and the masses and polar inertias per unit length of the members, in kg/m and kgm are, respectively 2×10^{-8} EA and 4×10^{-8} EI, with EA in N and EI in Nm^2

Member	Length (m)	EA (MN)	EI (Nm^2)	Tension (N)	Member	Length (m)	EA (MN)	EI (Nm^2)	Tension (N)
1	0.15	10	100	(−1.48)	11	(2.24)	0.14	0	5
2	(0.212)	10	100	0	12	(1.41)	0.14	0	5
3	0.15	10	100	0	13	1	3.2	10	(−25.8)
4	(0.362)	10	100	0	14	(1.73)	0.14	0	5
5	1	7	100	(−55.8)	15	(2.83)	0.14	0	5
6	1	7	100	(−70.1)	16	(8.25)	0.14	0	5
7	1	7	100	(−83.5)	17	2	3.2	10	(−9.50)
8	1	7	100	(−94.1)	18	(21.9)	0.14	0	5
9	(4.12)	0.14	0	5	19	(15)	0.14	0	5
10	(3.16)	0.14	0	5					

to replace its rigid body modes by tiny natural frequencies, which are then ignored. The principal structural elements are a regular polygonal ring with R_F (=6) sides, and a mast which is symmetric

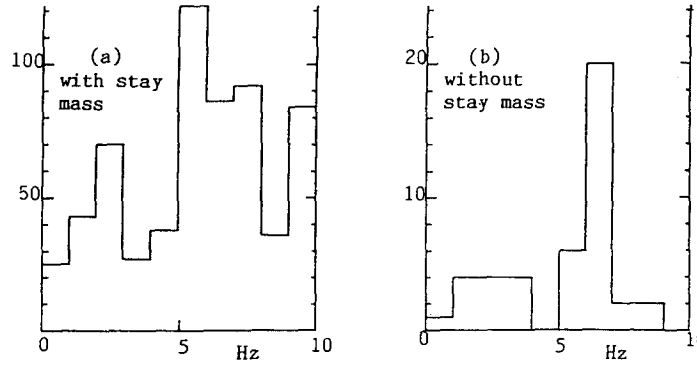

Fig. 8 Modal densities for the example of Table 1, using Eq. (17).

about the ring. Each side of the ring is a substructure, S_1, similar to that of Fig. 1(b) and with $R=R_1$ (=8) repeating portions. The mast consists of two identical compound stayed column substructures, S_3, with $R=R_3$ (=4) and which each contain two identical stayed columns, S_2, of the type shown in Fig. 1(c) with $R=R_2$ (=3). Every corner of the ring is connected by three pretensioned stays to the centre and ends of the mast.

Fig. 7 illustrates how the structure was represented when using BUNVIS-RG. The three substructures S_1-S_3 were modelled as class A substructures with S_2 within S_3, i.e., two level substructuring was used. Note that because class A substructures were used it was not necessary that $R_3=R_2$. For the repeating portions of rotationally periodic substructures (or of the final structure, F) shown on Fig. 7 the solid lines represent co-planar members and dashed lines are out-of-plane members. The members are numbered on the Fig. and their properties are given in Table 1, in which zero in the EI column denotes a stay; lengths in brackets are only approximate, but were calculated exactly from the geometry of the structure and the other lengths when preparing the BUNVIS-RG data; and similarly the tensions in brackets are only approximate, but BUNVIS-RG used the exact values calculated from the other tensions by statics, see below. (Those properties of Table 1 relating to the compound stayed column are modifications of a design presented previously by Jemah and Williams 1990).

Although the vibration analysis assumes all joints to be rigid, the static analysis assumed pinned joints and, for convenience, the relatively small axial force calculated for S_1 was shared equally between its longitudinal members, with the diagonal and ring members assumed to be unstressed. The tensions were all calculated to very high accuracy because otherwise the small out-of-balance forces at the joints imply the presence of small external loads at the joints, which can cause failure (Anderson and Williams 1987) of the BUNVIS-RG run if, loosely speaking, they are compressive across the structure, and large enough compared to the very small springs that suppress rigid body vibration modes for 'rigid body buckling' to occur.

The natural frequencies are numerous and many of the modes are almost exclusively dominated by the stays and so two actions were taken. Firstly, results were obtained ignoring stay masses, as well as accounting for them by exact taut wire theory. Secondly, most of the results are presented as modal densities, see Fig. 8, i.e., as the number of natural frequencies lying in a frequency interval, divided by the width of that interval. Because the frequency interval used is 1 Hz, the ordinate of Fig. 8 also gives the number of natural frequencies lying in each band.

Table 2 First nineteen natural frequencies, with stay masses omitted

No.	Hz	h	No.	Hz	h
1	0.5425	0	10	3.008	3
2,3	1.469	2	11	3.009	3
4,5	1.636	2	12	3.013	3
6	2.251	0	13	3.297	0
7	2.388	0	14,15	5.039	2
8	2.585	0	16,17	5.127	2
9	2.751	3	18,19	5.971	1

The theory presented is ideal for such calculations, by calculating J at each band boundary and subtracting.

It is obvious that the modes associated with most of the natural frequencies are dominated by the stays, since they are absent from Fig. 8(b), which excludes them. This method of seeing that the stays dominated the modes was preferred to using BUNVIS-RG to calculate the modes, to avoid the volume of results becoming excessive.

Table 2 gives the first nineteen natural frequencies for the massless stays case of Fig. 8(b). The six obvious 'rigid body' frequencies are excluded, as is a seventh zero frequency mode which occurs because the stays of Fig. 6 cannot prevent relative rotation of the mast and the ring. (This seventh zero frequency mode was accepted to keep the example reasonably simple, but would be eliminated in practice, e.g., by including 'hubs' at the top and bottom of the mast and replacing the stays of Fig. 6 by ones arranged like the spokes of a bicycle wheel).

It took about 25 CPU mins on a MicroVAX 3900 computer to find Fig. 8(a) and about 4 CPU mins to find a single individual natural frequency. Therefore it would have been prohibitive to demonstrate the computational efficiency of the multi-level rotationally periodic substructuring by performing runs that did not use it. However, use of an appropriate formula for predicting BUNVIS-RG computation times (Anderson and Williams 1987) indicates that the solution would have taken about 500 times longer if neither the rotationally periodic nature of the parent structure nor of its substructures had been used, so that the whole structure would have been modelled without substructuring. If class B substructuring had been implemented in BUNVIS-RG, its use with the multi-level doubling up of substructures described in the Introduction in connection with Fig. 1(b), i.e., substructure S_1, would have reduced the solution time by a factor of about ten, i.e., Fig. 8(a) would have required about 3 VAX CPU mins.

6. Other forms of repetition

Based on earlier work (Anderson 1981), theory within BUNVIS-RG covers frames that are repetitive in one, two or three Cartesian directions. Exact finite elements are again permitted, by including an Eq. analogous to Eq. (19). The size of the problem analysed is that of the repeating portion of the frame. Briefly, the method requires that the response mode is repetitive over N_1, N_2 and N_3 bays in the three coordinate directions, such that

$$\boldsymbol{D}_j = \boldsymbol{D}_0 \exp\{2i\pi(n_1 j_1/N_1 + n_2 j_2/N_2 + n_3 j_3/N_3)\} \tag{34}$$

where $\boldsymbol{D}_j$ is the (complex) displacement amplitude vector of the j-th repeating portion, which is separated from the datum repeating portion by j_1, j_2 and j_3 bays in the three coordinate directions.

7. Conclusions

The Abstract may be read as a summary of the principal conclusions.

References

Anderson, M.S. (1981), "Buckling of periodic lattice structures", *AIAA J.*, **19**(6), 782-788.

Anderson, M.S. (1982), "Vibration of prestressed periodic lattice structures", *AIAA J.*, **20**(4), 551-555.

Anderson, M.S. and Williams, F.W. (1986), "Natural vibration and buckling of general periodic lattice structures", *AIAA J.*, **24**(1), 163-169.

Anderson, M.S. and Williams, F.W. (1987), "BUNVIS-RG: Exact frame buckling and vibration program, with repetitive geometry and substructuring", *J. Spacecraft and Rockets*, **24**(4), 353-361.

Balasubramanian, P., Suhas, H.K. and Ramamurti, V. (1991), "Skyline solver for the static analysis of cyclic symmetric structures", *Comp. and Struct.*, **38**(3), 259-268.

Capron, M.D. and Williams, F.W. (1988), "Exact dynamic stiffnesses for an axially loaded uniform Timoshenko member embedded in an elastic medium", *J. Sound Vib.*, **124**(3), 453-466.

Capron, M.D., Williams, F.W. and Symons, M.V. (1987), "A parametric study of the free vibrations of an offshore structure with piled foundations", *Proc. Int. Conf. on Steel and Alum. Structs.: Steel Structs.*, Cardiff, 653-664. (Elsevier Applied Science, London).

Henry, R. and Ferraris, G. (1983), "Substructuring and wave propagation: an efficient technique for impeller dynamic analysis", *ASME Trans.*, Paper No. 83-GT-150, *28th Int. Gas Turbine Conf. and Exhibit*, Phoenix, Arizona, 27-31 March.

Howson, W.P., Banerjee, J.R. and Williams, F.W. (1983), "Concise equations and program for exact eigensolutions of plane frames including member shear", *Adv. Eng. Software*, **5**(3), 137-141.

Jemah, A.K. and Williams F.W. (1990), "Compound stayed column for use in space", *Comp. and Struct.*, **34**(1), 171-178.

Leung, A.Y.T. (1980), "Dynamic analysis of periodic structures", *J. Sound Vib.*, **72**(4), 451-467.

Lundén, R. and Åkesson, B.A. (1983), "Damped second-order Rayleigh-Timoshenko beam vibration in space-an exact complex dynamic member stiffness matrix", *Int. J. Num. Meth. Engng.* **19**(3), 431-449.

MacNeal, R.H., Harder, R.L. and Mason, J.B. (1973), "NASTRAN cyclic symmetry capability", NASTRAN User's Experience-3rd Coll., NASA TM X-2893, 395-421.

McDaniel, T.J. and Chang, K.J. (1980), "Dynamics of rotationally periodic large space structures", *J. Sound Vib.*, **68**(3), 351-368.

Thomas, D.L. (1979), "Dynamics of rotationally periodic structures", *Int. J. Num. Meth. Engng.* **14**(1), 81-102.

Wildheim, S.J. (1981), "Dynamics of circumferentially periodic structures", Doctoral Thesis, Linköping Univ., Sweden.

Williams, F.W. (1986a), "An algorithm for exact eigenvalue calculations for rotationally periodic structures", *Int. J. Num. Meth. Engng.* **23**(4), 609-622.

Williams, F.W. (1986b), "Exact eigenvalue calculations for structures with rotationally periodic substructures", *Int. J. Num. Meth. Engng.* **23**(4), 695-706.

Williams, F.W. and Wittrick, W.H. (1983), "Exact buckling and frequency calculations surveyed", *J. Struct. Engng ASCE*, **109**(1), 169-187.

Wittrick, W.H. and Williams, F.W. (1971), "A general algorithm for computing natural frequencies of elastic structures", *Q.J. Mech. Appl. Math.*, **24**(3), 263-284.

Wittrick, W.H. and Williams, F.W. (1973a), "An algorithm for computing critical buckling loads of elastic structures", *J. Struct. Mech.*, **1**(4), 497-518.

Wittrick, W.H. and Williams, F.W. (1973b), "New procedures for structural eigenvalue calculations", *4th Australasian Conf. on the Mechanics of Structures and Materials*, U. of Queensland, Brisbane, Queensland, Australia, 299-308.